

Spiral Readout Gradients for the Reduction of Motion Artifacts in Chemical Shift Imaging

Dong-Hyun Kim,^{1,2*} Elfar Adalsteinsson,¹ and Daniel M. Spielman¹

A motion artifact reduction method for proton chemical shift imaging (CSI) is presented. The method uses spiral-based readout gradients for data acquisition. A characteristic of spiral-based readout gradients is that data are repeatedly sampled at the k_{xy} origin. These data points are used to estimate and correct for motion-induced phase variations. Both phantom and in vivo spectra reconstructed using the new motion artifact reduction algorithm showed significant signal-to-noise ratio (SNR) improvements as compared to uncorrected data. Magn Reson Med 51:458–463, 2004. © 2004 Wiley-Liss, Inc.

Key words: motion artifact reduction; spiral CSI

Chemical shift imaging (CSI) provides both metabolic and spatial information from the metabolites of interest. To date, the vast majority of CSI applications have focused on the brain. However, studies outside of the brain, including prostate (1) and breast (2), suggest an important role for CSI in differentiating between cancer, necrosis, and normal tissue. Single-voxel ^1H spectroscopy studies in other organs indicate that the application of CSI to these regions may have clinical value (3–5). A major technical challenge for CSI studies, particularly for non-brain tissues, comes from the presence of cardiac and respiratory motion, which leads to various forms of artifacts (6).

The presence of motion during a single-voxel spectroscopy study can lead to a variety of artifacts. Averaging each acquisition, which is commonly used to obtain sufficient SNR, can lead to decreased signal intensity due to the view-to-view incoherences. The main sources of view-to-view incoherences come from the different phase and amplitudes acquired during each acquisition. For example, gradients applied during excitation give rise to phase accumulation that is proportional to motion. In particular, crusher gradients applied to suppress unwanted signal from spins can be highly sensitive to motion. Another artifact is the presence of motion during the relatively long readout time of spectroscopic studies, which can lead to spectral line-broadening due to time varying frequency shifts caused by dynamic magnetic field changes.

Previously proposed motion correction schemes for single-voxel spectroscopy have relied on the fact that one can manipulate each individual readout prior to averaging. Zero-order phasing of each acquisition prior to averaging can recover the signal intensity loss, while frequency shifts caused by magnetic field changes can be recovered by applying a first-order (linear) phase to the data, thereby reducing the line-broadening (7). In both cases, an adequate SNR signal (e.g., from water) is required so that robust phasing can be performed (8). These correction methods for single-voxel studies have been applied not only to the brain but also to other organs where motion can be severe (9). The application of zero-order and first-order phasing therefore reduces phase changes that are due to motion. This will result in aligning each acquisition in terms of phase, which will ultimately increase the SNR of the exam.

For normal phase-encoded CSI studies, the above phasing methods cannot be directly applied because phase-encoding gradients are used prior to readout to encode spatial information. In addition to the artifacts mentioned above, for CSI, ghosting, which is a commonly observed motion artifact in other MR imaging applications, can also be present. To overcome these problems, Posse et al. (10) introduced a method where phase-encoding gradients occur after starting the readout in order to acquire the information needed for zero-order phasing. They also used moment compensated gradients during the excitation period to minimize motion effects occurring during this period. Other methods for reduced motion artifacts in CSI applications include using reference markers (11) and navigators (12). These methods, however, depend on the use of phase-encoding gradients for the acquisition of CSI data, which can be susceptible to motion artifacts similar to artifacts found in 2D Fourier transform (2DFT) imaging scans (13).

In this article, we present a new motion artifact reduction method for CSI which uses spiral-based readout gradients. This method corrects for motion in an analogous manner to that used in conventional single-voxel spectroscopy, enabling both zero-order and first-order phase corrections. The algorithm corrects for phase changes from inter-view motion as well as phase changes during the readout due to intra-view motion. We first present the basic idea of the method, followed by the implementation. Phantom and in vivo results are given to illustrate the improved data quality when the algorithm is used.

SPIRAL-BASED READOUT GRADIENT SEQUENCE

The basic idea behind using spiral-based readout gradients for CSI motion artifact reduction comes from the k -space

¹Radiological Sciences Laboratory, Department of Radiology, Stanford University, Stanford, California.

²Department of Electrical Engineering, Stanford University, Stanford, California.

Grant sponsors: GE Medical systems, NIH; Grant numbers: CA 48269, RR09784, AG 18942.

*Correspondence to: Dong-hyun Kim, Lucas MRS Imaging Center, Stanford CA 94305-5488. E-mail: dhkim@stanford.edu

Received 13 January 2003; revised 17 October 2003; accepted 20 October 2003.

DOI 10.1002/mrm.20004

Published online in Wiley InterScience (www.interscience.wiley.com).

© 2004 Wiley-Liss, Inc.

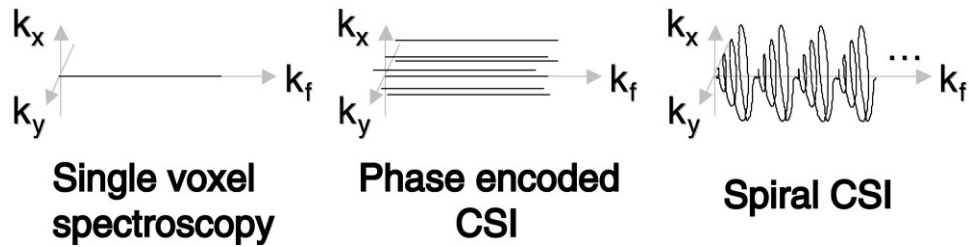


FIG. 1. A comparison of the k -space sampling schemes for single-voxel spectroscopy, conventional phase-encoded CSI, and spiral CSI. The similarity between single-voxel spectroscopy and spiral CSI can be readily seen from this figure. Spiral CSI is designed so that the spiral lobes are repeatedly rewound back to $k_{xy} = 0$, which is also the case of single-voxel spectroscopy where continuous samples of $k_{xy} = 0$ are collected. This feature is the basis for the algorithm.

sampling scheme of the sequence (Fig. 1). The sequence acquires k_{xy} spatial data in a spiral fashion (14). At the end of each spiral waveform is a rewinding lobe that brings the trajectory back to the k_{xy} origin. To obtain spectral information, the spiral and rewinding waveforms are repeated throughout the readout. Due to this k -space sampling scheme, the spiral CSI sequence has the characteristic of repeatedly sampling the k_{xy} origin. The data points corresponding to $k_{xy} = 0$ have no phase-encoded spatial information and can thus be extracted for phase correction. This scheme is similar to single-voxel spectroscopy where data acquisition can be regarded as collecting only $k_{xy} = 0$ points and correcting for any motion-induced phase changes. Figure 1 illustrates the similarity in the sampling scheme between single-voxel spectroscopy and spiral CSI. As shown in the figure, k_{xy} origin data are repeatedly collected for the two methods, whereas traditional phase-encoded CSI acquires k_{xy} origin data for only one of the many acquisitions. Our motion artifact reduction method is therefore based on this similar sampling scheme between the two acquisitions.

The spiral CSI sequence is also characterized by a reduced minimum total measurement time, which is the minimum time required to sample the whole k -space (15). This time is significantly reduced compared to normal phase-encoded CSI sequences, in which a minimum of one repetition time (TR) is necessary for each resolved voxel. For example, given our current gradient hardware (4 G/cm, 15 G/cm/ms), the minimum total measurement time for a spiral CSI sequence using a 20 cm field of view (FOV) which covers a 32×32 matrix with ~ 400 Hz spectral bandwidth can be acquired in four TRs using four spatial interleaves. Figure 2 illustrates the spatial interleaving of the spirals and also the sampling in the k_f dimension. Note

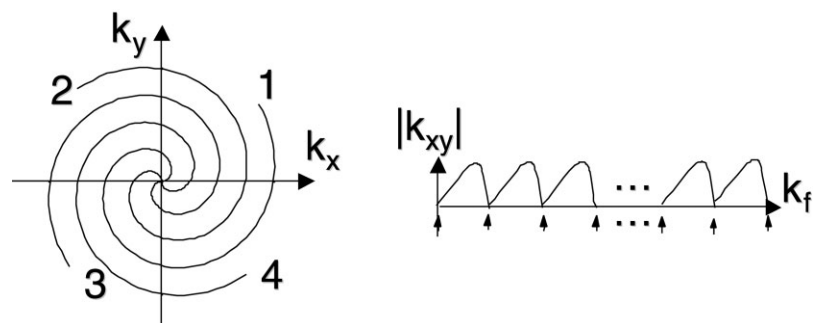
that even though different spatial interleaves correspond to different spatial encoding, all these trajectories sample the $k_{xy} = 0$ points repeatedly and the samples taken can therefore be treated as equivalent data points in terms of k_{xy} versus k_f . Since the minimum total measurement time is short compared to normal phase-encoded CSI, many acquisitions are used to gain equivalent SNR. Multiple acquisitions can also reduce the artifacts coming from motion since gross effects are compensated when averaged (16).

In addition, spiral-based readout gradients in imaging applications have been found to be superior both in terms of efficiency and insensitivity to motion compared to 2DFT scans due to gradient moment nulling effects (13). A velocity k -space analysis shows that spiral sequences are immune to many flow effects as well (17). Therefore, combining these advantageous characteristics of the spirals with the proposed phase correction scheme could significantly improve the quality of in vivo spectra when motion-induced phase artifacts are present.

MATERIALS AND METHODS

To illustrate the reduced motion artifacts of our proposed method, we developed a pulse sequence with the following characteristics. We incorporated spiral-based readout gradients into the PRESS (point resolved spectroscopy) sequence (18) and designed the spirals using a simple analytic design algorithm (19) which enables a flexible real-time design (1.5 T GE Signa LX). Rewinding gradients, which bring back the k -space trajectory to the origin, were added at the end of each spiral to connect consecutive spiral lobes. For phantom and in vivo brain studies, 4 k_{xy} spatial interleaves over a 20-cm FOV covering a 32×32

FIG. 2. An example of the spiral trajectory for a four k_{xy} interleave design. Although each readout interval is interleaved with spirals rotated by 90° (left), in terms of $|k_{xy}|$ and k_f , the trajectory is kept the same, as shown (right). Therefore, all data points extracted from $k_{xy} = 0$ can be treated as being free of phase variations imposed by the spatial localization.



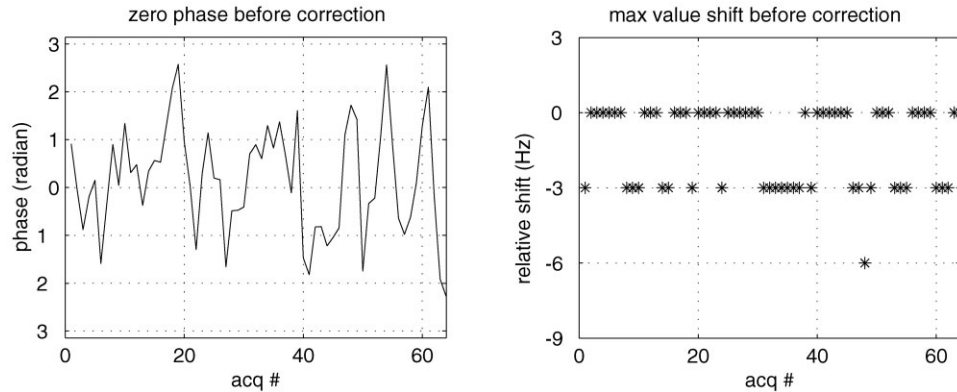


FIG. 3. Phase of the initial points of each acquisition (excitation) from the motion-induced phantom before the zero-order phase correction is applied (left). Relative shift of water resonance, which determines the amount of first-order phase to be applied, for each acquisition before the correction is applied (right).

matrix were used while data were collected with a standard head coil. This trajectory achieves spectral bandwidth of ~ 400 Hz (2.5 ms spiral lobe). The spirals were repeated 134 times during the 320-ms readout interval (TR/TE = 1500/144 ms, gradient hardware: 4 G/cm, 15 G/cm/ms). To gain sufficient SNR, we obtained multiple acquisitions so that the total scan times were equivalent to the cases of a 32×32 phase-encoded CSI study. The water suppression was adjusted so that sufficient residual water was available for phasing, and to keep all metabolites in-phase we began data acquisition at the echo time, i.e., when the k_{xyf} value is zero.

After acquiring the data, we took the following steps to correct for motion-induced artifacts. We extracted the data points corresponding to $k_{xy} = 0$ from each interleaf of each acquisition. The amount of zero-order phase was estimated from the initial point ($k_{xyf} = 0$) of the data and applied to the whole raw data. For first-order phasing, the position of the water peak from the spectrum was estimated after Fourier transform of each extracted data frame from an acquisition. We then calculated an average position of the peak from all the peak positions and applied first-order phase correction corresponding to this average shift to the raw data. Following this correction step, we used gridding to reconstruct the data.

We applied the above correction algorithm to both phantom and in vivo cases. For phantom experiments, data were acquired from a spherical MR spectro phantom which contains metabolite solutions similar to in vivo brain: NAA (12.5 mM), Cr (10.0 mM), Cho (3.0 mM), and lactate (5 mM). We induced motion by gently rocking the phantom as if it were experiencing respiratory movement. In this case, the movement was constrained to ~ 1.5 cm with a period of ~ 5 sec. Occasional irregularities were also added. The direction of movement was not restricted. The phase and amplitude variations from each acquisitions were measured to estimate the amount of motion. We then acquired in vivo brain spectra from a healthy volunteer. In this case, data were acquired both with the volunteer lying still by adding foams to rigidly constrain the head and with the volunteer free to move by removing the foams. The volunteer was asked to move similar to the movement induced on the phantom. The direction of motion was mostly constrained to be in-plane. This study design enables comparison of data with and without motion, which is useful for evaluating our method in in vivo cases. For all

in vivo studies as well, the phase and amplitude variations were calculated for an estimate of motion.

Finally, we evaluated the difference in the k -space trajectories between the prescribed trajectory and the actual trajectory being played out by using a measurement method presented by Alley et al. (20). Due to imperfect gradient design and eddy current effects, the trajectory might not follow the exact path being prescribed, which can lead to errors when the phasing technique is applied.

RESULTS

We now demonstrate that our algorithm improves the SNR by providing the experimental results. Figures 3 and 4 display data acquired from a spherical MR spectro phantom with gentle movement. In Fig. 3, the amount of phase discrepancy due to motion for each acquisition (excitation) before the zero-order phase correction is displayed in the first column. The second column shows the relative frequency shifts of the water peak after Fourier transforming the extracted $k_{xy} = 0$ data from each acquisition before first-order phase correction. The plots give a reference of how much motion was actually induced during the experiment. The amount of phase variation from the acquisitions was ± 2.20 radians and the amplitude variation was $\pm 3.4\%$ after normalizing the magnitude of the amplitude. The algorithm reduces the dispersion of the phase (zero- and first-order) from each individual interleaf. Figure 4 displays representative spectra extracted from the reconstructed matrix and within the PRESS box shown for different cases. As shown in Fig. 4, the application of the motion artifact reduction algorithm enhances the spectral quality as well as reducing the spatial artifacts outside of the excited region. The SNR of the NAA metabolite was calculated by measuring the height of the of the NAA signal and dividing by two times the standard deviation of signal from the range where no metabolites existed (21), namely, from the 6–8 ppm region. The relative SNR from the central 8×8 spectra for each experiment was 0.18 (± 0.02) with no motion correction, 0.79 (± 0.05) with motion correction, and 1.0 (± 0.08) with no motion.

Figure 5 displays data obtained from an in vivo brain and three representative spectra from the reconstructed 16×16 matrix for each experiment. The amount of phase and amplitude variation from motion was calculated to be ± 1.45 radians and $\pm 32\%$ after normalizing, respectively.

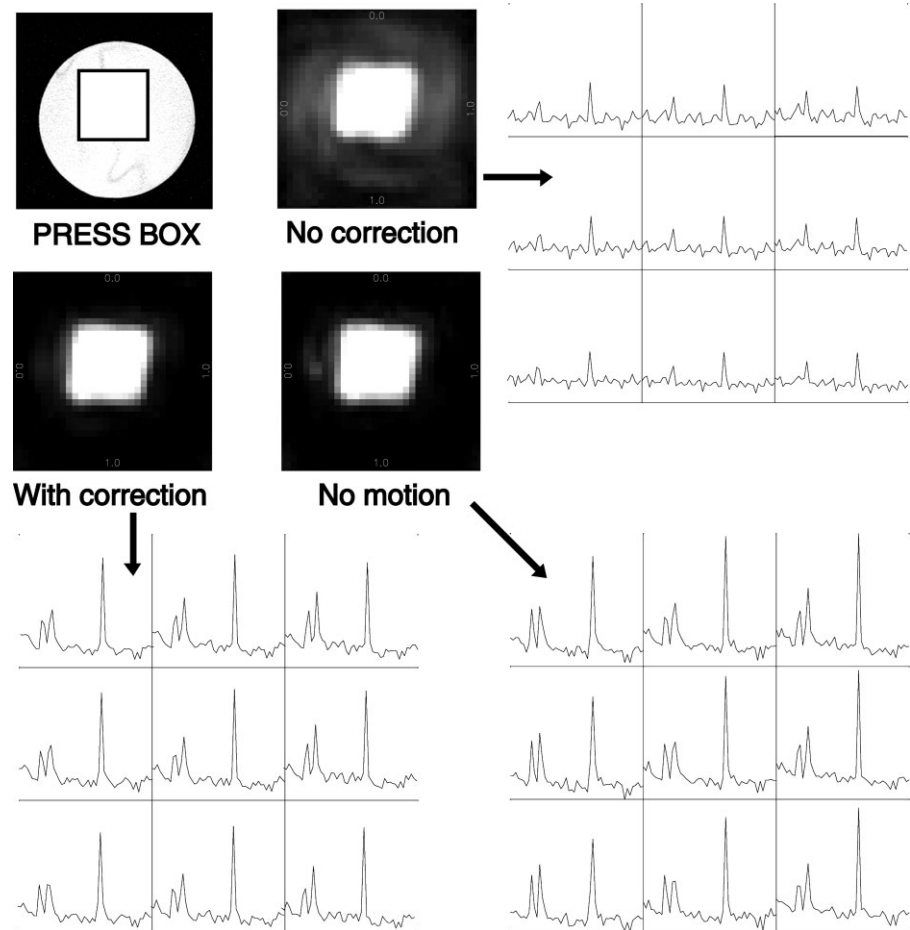


FIG. 4. Results from the phantom study. The reference water image and the corresponding PRESS box selection is displayed at the top left. Also, reconstructed water images from the spiral CSI acquisition are displayed from various algorithms applied. As can be seen, blurring of the image is observed when no correction is applied. Extracted spectra from the 32×32 reconstructed matrix are also displayed. The enhanced spectral quality is readily observed when the motion reduction algorithm is applied. Relative metabolite SNR of the NAA peak for each method was 0.18: no correction with motion, 0.79: with correction with motion, and 1.0: with no motion.

The relative SNR of the residual water resonance, calculated similarly to the SNR calculation from the phantom experiment, was $0.73 (\pm 0.09)$ with no motion correction, $0.89 (\pm 0.16)$ with motion correction, and $1.0 (\pm 0.25)$ with negligible motion by holding the subject's head rigidly in place. Sixteen voxels from the center were used for calculation of the SNRs.

Finally, Fig. 6 overlays the calculated and the measured trajectory for the first spiral lobe of the readout. As demonstrated, there is a small difference between the two, which can accumulate during the long readout time of a CSI sequence. Nevertheless, we have found experimentally that this does not significantly affect the performance of the algorithm, since most of the energy of the data are concentrated at the beginning of the readout time ($=TE$) where the degree of drift is insignificant.

DISCUSSION

We have demonstrated a motion artifact reduction method for CSI based on spiral readout gradients and have shown that, with the reduction method, increased SNR of metabolites of interest can be achieved. Previously, spiral CSI has been shown to have flexible resolution vs. scan time properties (14), which can significantly reduce the minimum total measurement time compared to normal phase-encoded methods. Therefore, multiple acquisitions of the same k -space data can be achieved within the same scan

time, which alone allows reduction of motion artifacts. In this article we have shown that we can further reduce motion artifacts by applying phasing techniques to data points extracted from the k_{xy} origin, thereby increasing the SNR of the metabolite spectrum.

The algorithm corrects for phase discrepancies at the start of and during the readout due to motion. Therefore, any motion effects that give rise to phase discrepancies can be corrected. As seen from the experiments, the higher the variations of phase due to motion, ± 2.20 radians for phantom exam and ± 1.45 radians for head exam, the phase correction resulted in better SNR improvements. On the other hand, phase discrepancies are not the only artifacts that arise from motion. For example, motion can induce variation in the amplitude from each acquisition, $\pm 3.4\%$ for phantom exam and $\pm 32\%$ for head exam. Correction based on amplitude variations could also have been implemented along with the phasing method. In our studies, the head exam had significant amplitude variation; therefore, it could have benefited from amplitude corrections. Alternatively, since amplitude correction can deteriorate the spectra by enhancing the noise level instead, methods based on acceptance/rejection can also be used (22). In summary, motion will give rise to various artifacts, and in this study we corrected for phase variations that arise due to motion.

The use of the spiral-based trajectories plays an important role for the proposed method. The ability to phase

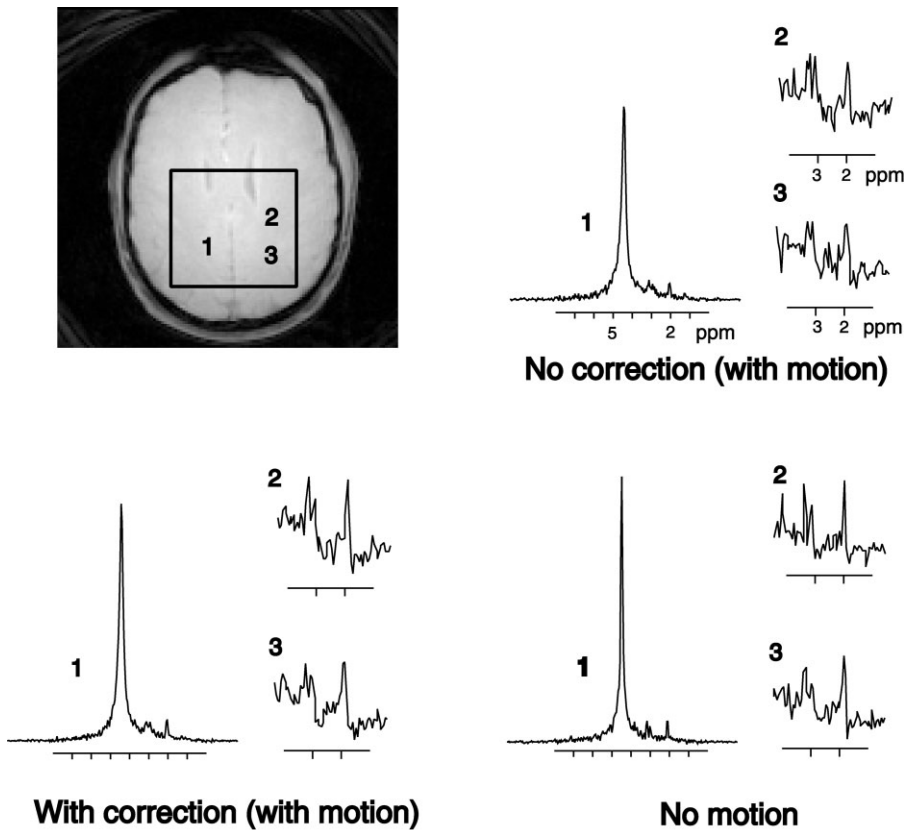


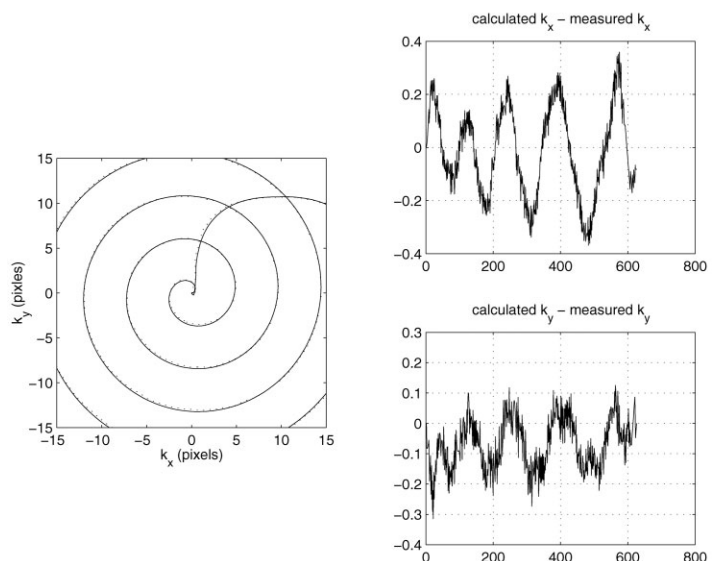
FIG. 5. Results from a volunteer head exam. In this exam, 16×16 spectra were reconstructed and representative spectra from the image are displayed here. In voxel 1, the whole spectral bandwidth is displayed, while voxels 2 and 3 focus on 1–4 ppm region. Relative SNR of the reconstructed water from 16 voxels were 0.73: no correction with motion, 0.89: with correction with motion, and 1.0: with no motion.

each individual data acquisition depends on the fact that every readout samples the same k_{xy} origin at the same k_f points. Previously, spectral and spatial interleaves were used to cover the desired bandwidth. For spectral interleaves, not all samples from the k_{xy} origin correspond to the same k_f point. In our method, we therefore eliminated all spectral interleaves and applied only spatial interleaves instead. This ensures that all data points sampled at the k_{xy} origin are at the same k_f points for all interleaves. Increased spectral bandwidth can be achieved by increas-

ing the number of spatial interleaves of the spirals, which might be needed, e.g., for higher field strength system applications.

Several factors may limit the application of our proposed method. The first of these involves the accuracy of the spirals in tracing the desired k -space trajectory. In particular, the trajectory's ability to rewind back to the k_{xy} origin between successive spiral lobes is crucial when applying the first-order phase correction, as demonstrated in Fig. 6. Due to imperfect gradient design or eddy current

FIG. 6. Spiral trajectory measurement using the method mentioned. A disparity in the calculated trajectory (solid line) and the measured trajectory (dotted line) exists which can lead to problems since the spirals are repeated throughout the readout interval (left). Nevertheless, the amount of disparity is not a significant effect since most of the energy in the obtained data are concentrated during the early part of the readout. The disparity is also plotted on the right for each axis using the same scale as on the left (right top: X axis, right bottom: Y axis).



effects, the trajectory may not exactly rewind back to the origin. Although the amount of drift is insignificant in our implementations, careful measurement and correction of the spiral trajectory must precede the application of first-order phasing when the degree of drift is significant. For example, rewinders can be designed so that there is a compensation factor to first order in the trajectory against the drift.

This method is currently limited to motion artifact reduction in two-dimensional situations. A natural expansion of this work would be to have the capability for 3D CSI applications. In essence, 3D applications are feasible as long as repeated sampling of the k_{xyz} origin exists, thereby allowing the phasing techniques. There are many alternative ways to achieve repeated sampling of the k_{xyz} origin. We might, for example, use multislice acquisitions where each slice repeatedly samples k_{xy} origin. We can also achieve repeated sampling by building more elegant readout trajectories (23). As a simple example, since phase-encoding in the third dimension is conventionally used for 3D acquisitions, we can temporarily rewind the phase-encoded gradients back to the origin while the spirals are rewinding, creating a readout trajectory that samples k_{xyz} origin repeatedly. These and various other methods could allow us to expand our algorithm to 3D applications.

Finally, to phase the data there needs to be a sufficient SNR in the acquired samples. In our method we achieved this by first sampling at the echo time where the signal level is highest. We also set the water suppression at an appropriate level to ensure a sufficient residual water signal (~10:1 for water:metabolite). An alternative method for maintaining an adequate SNR level would be to have better control of the excitation profile. For example, Starlack et al. (8) introduced a dual-band excitation profile which suppresses the lipids while maintaining the suppressed water at a desired level for signal phasing. These profiles can be used in our spiral PRESS sequence to establish better control of metabolite and reference signal levels.

CONCLUSION

In the above study, we presented a method for motion artifact reduction of 2D proton CSI. The method uses the characteristic of spiral-based readout gradients which repeatedly sample the k_{xy} space origin. It does not require additional data acquisition nor separate navigator echoes and can be implemented as a simple postprocessing scheme. Phantom and in vivo data illustrate the improved spectral quality when the method is applied.

REFERENCES

1. Kurhanewicz J, Vigneron, DB, Hricak H, Narayan P, Carroll P, Nelson SJ. Three-dimensional ^1H MR spectroscopic imaging of the in situ human prostate with high (0.24-0.7 cm³) spatial resolution. *Radiology* 1996;198:795–805.
2. Spielman DM, Hunjan S, Glover AS, Adalsteinsson E, Ikeda DM. Proton spectroscopic imaging of breast cancer. In: Proc 9th Scientific Meeting ISMRM, Glasgow, 2001. p 2323.
3. Kim DY, Kim MY, Kim GD, Kim JK. Localized in vivo proton spectroscopy of renal cell carcinoma in human kidney. *J Korean Med Sci* 1998;13:49–53.
4. Tyszka JM, Silverman JM. Navigated single-voxel proton spectroscopy of the human liver. *Magn Reson Med* 1998;39:1–5.
5. Starlack JM, Spielman DM, Adalsteinsson E, Kurhanewicz J, Vigneron DB. In vivo lactate editing with simultaneous detection of choline, creatine, NAA, and lipid singlets at 1.5T using PRESS excitation with applications to the study of brain and head and neck. *J Magn Reson* 1998;133:243–254.
6. Felblinger J, Kreis R, Boesch C. Effects of physiologic motion of the human brain upon quantitative ^1H -MRS: analysis and correction by retro-gating. *NMR Biomed* 1998;11:107–114.
7. Helms G, Piringer A. Restoration of motion-related signal loss and line-shape deterioration of proton MR spectra using the residual water as intrinsic reference. *Magn Reson Med* 2001;46:395–400.
8. Starlack JM, Adalsteinsson E, Gold GE, Ikeda DM, Spielman DM. Motion correction and lipid suppression for ^1H magnetic resonance spectroscopy. *Magn Reson Med* 2000;43:325–330.
9. Bolan P, DeLaBarre L, Baker E, Merkle H, Everson L, Yee D, Garwood M. Correcting respiratory-induced frequency shifts in breast MRS at high field. In: Proc 10th Scientific Meeting ISMRM, Honolulu, 2002. p 2516.
10. Posse S, Cuenod CH, LeBihan D. Motion artifact compensation in ^1H spectroscopic imaging by signal tracking. *J Magn Reson* 1993;102:222–227.
11. Haupt CI, Kiefer AP, Maudsley AA. In plane motion correction for MR spectroscopic imaging. *Magn Reson Med* 1998;39:749–753.
12. VanDerVeen J, Weinberger D, Duyn J. Navigator corrections in proton spectroscopic imaging. In: Proc 10th Scientific Meeting ISMRM, Honolulu, 2002. p 2517.
13. Glover GH, Lee AT. Motion artifacts in fMRI: comparison of 2DFT and PR and spiral scan methods. *Magn Reson Med* 1995;33:624–635.
14. Adalsteinsson E, Irazzabal P, Topp S, Meyer C, Macovski A, Spielman DM. Volumetric spectroscopic imaging with spiral-based k -space trajectories. *Magn Reson Med* 1998;39:889–898.
15. Twieg DB, Katz J, Peshock RM. A general treatment of NMR imaging with chemical shifts and motion. *Magn Reson Med* 1987;5:32–46.
16. Ebel A, Maudsley A. Comparison of methods for reduction of lipid contamination for in vivo proton MR spectroscopic imaging of the brain. *Magn Reson Med* 2001;46:706–712.
17. Nishimura DG, Irarrazabal P, Meyer CH. A velocity k -space analysis of flow effects in echo-planar and spiral imaging. *Magn Reson Med* 1995;33:549–556.
18. Bottomley PA. Spatial localization in NMR spectroscopy in-vivo. *Ann NY Acad Sci* 1987;508:333–348.
19. Glover GH. Simple analytic spiral k -space algorithm. *Magn Reson Med* 1999;42:412–415.
20. Alley MT, Glover GH, Pelc NJ. Gradient characterization using a Fourier transform technique. *Magn Reson Med* 1998;39:581–587.
21. Freeman R. A handbook of nuclear magnetic resonance, 2nd ed. London: Longman; 1997.
22. Sachs TS, Meyers CH, Irarrazabal P, Hu BS, Nishimura DG, Macovski A. The diminishing variance algorithm for real-time reduction of motion artifacts in MRI. *Magn Reson Med* 1995;34:412–422.
23. Irarrazabal P, Nishimura DG. Fast three dimensional magnetic resonance imaging. *Magn Reson Med* 1995;33:656–662.